Journal of the Optical Society of America B
OPTICAL PHYSICS

Sub-microwave wavelength localization of Rydberg superatoms

Rahmatullah,[1,2,*] Ziauddin,[1,2] You-Lin Chuang,[1,3] Ray-Kuang Lee,[1,3,4] and Sajid Qamar[2,5]

[1]Institute of Photonics Technologies, National Tsing Hua University, Hsinchu 300, Taiwan
[2]Quantum Optics Laboratory, Department of Physics, COMSATS University, Islamabad, Pakistan
[3]Physics Division, National Center for Theoretical Sciences, Hsinchu, Taiwan
[4]e-mail: rklee@ee.nthu.edu.tw
[5]e-mail: sajid_qamar@comsats.edu.pk
*Corresponding author: rahmatktk@comsats.edu.pk

Received 11 May 2018; revised 15 July 2018; accepted 24 August 2018; posted 29 August 2018 (Doc. ID 331527); published 24 September 2018

With the interaction among one optical probe field and pairs of standing microwaves in the configuration of Rydberg-dressed electromagnetically induced transparency, we study theoretically the sub-microwave wavelength localization of Rydberg superatoms in two and three dimensions. Composited by an ensemble of Rydberg atoms with strong dipole–dipole interactions, a superatom can be localized within the microwave wavelength through the position-dependent atom–field interaction. By measuring the absorption spectrum from the optical probe field, a single position of Rydberg superatoms with high precision can be obtained, depending on the probe field detuning and phase shifts associated with the standing microwaves.

https://doi.org/10.1364/JOSAB.35.002588

1. INTRODUCTION

With potential applications as the atom–light interfaces for quantum information processing, Rydberg atoms have demonstrated remarkable properties such as long excitation lifetime and large polarizability [1–11]. Due to the dipole blockade effect, i.e., suppression in the excitations of more than one atom into Rydberg state, *superatoms* can be formed within a large volume [12–15]. These superatoms account for the collective enhancement of Rabi oscillations in multiple or single pairs of atoms [16–18], which can be further excited at the single photon level [19–21]. Moreover, the Rydberg ensemble as a whole can also be excited in the crystalline structures with chirped laser pulses [22].

Similar to neutral atomic systems of electromagnetically induced transparency (EIT), Rydberg-dressed EIT has attracted much attention over the last decade both experimentally and theoretically, due to the strong, long-range interactions among Rydberg atoms [23–28,15]. In particular, Petrosyan and Fleischhauer developed a theory to study EIT in an ensemble of strongly interacting Rydberg atoms with the mean-field approximation by introducing two-photon correlations [26]. When each superatom has at most one Rydberg excitation within the blockade volume, such a coarse-grained treatment on an ensemble of superatoms is valid within the weak probe-field approximation [27]. These Rydberg superatoms can also be used to realize parity-time ($\mathcal{PT}$)-symmetry in atomic systems [29], or coupled to hybrid optomechanical systems [30,31].

In this work, we propose a scheme for the atomic localization of Rydberg superatoms in two dimensions (2D) and three dimensions (3D). As the size of Rydberg superatoms is in the unit of micrometers, we use standing microwaves to confine superatoms, but reveal the precision in atomic localization to the sub-optical wavelength of the probe field. Even though the idea to use standing waves has already been applied for atomic localization at the sub-wavelength scale for the one-dimensional setting [32–40], as well as for 2D [41–49] and 3D space [50–53], until now only a single atom has been studied. Here, we consider the localization of an ensemble of Rydberg atoms with a strong dipole–dipole interaction in 2D and 3D space. In the 2D setting, we consider that the Rydberg superatom is interacting with the superposition of two pairs of orthogonal standing microwaves acting along the x- and y-directions, while in 3D, the superatom interacts with three pairs of orthogonal standing microwaves aligned in the x-, y-, and z-directions, respectively. The information about the position of one superatom can be obtained by measuring the absorption spectrum from the optical probe field. We show that within a microwave wavelength, one can obtain the position information of the Rydberg superatom through the frequency detuning and phase shifts of the probe field.

2. THEORETICAL MODEL

We consider an ensemble of cold ^{87}Rb atoms with allowed transitions in the cascade configuration, through the interaction with the probe and control fields, as shown in Fig. 1(a).

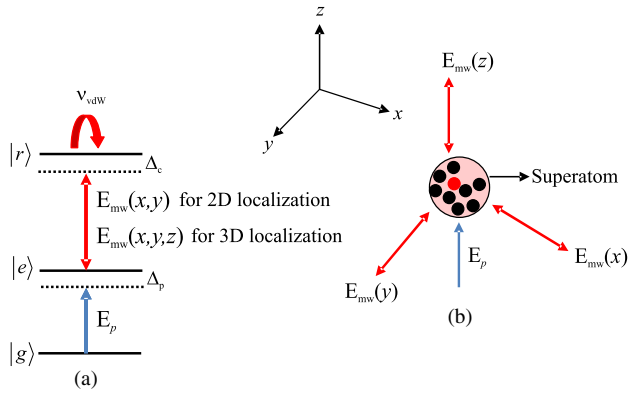

Fig. 1. Schematics for our scheme to realize the localization of Rydberg superatoms at sub-microwave wavelength. (a) The intermediate state $|e\rangle$ is coupled to the ground state $|g\rangle$ and highly excited Rydberg state $|r\rangle$ via a weak optical probe field E_p and pairs of standing microwave fields $E_{mw}(l)$, $l = x, y$, and $l = x, y, z$ for 2D and 3D localizations, respectively. Here, $\mathcal{V}_{\rm vdW}$ represents the van der Waals interaction between the atoms in the Rydberg state $|r\rangle$. (b) Illustration of 3D localization with three standing-wave fields $E_{mw}(x)$, $E_{mw}(y)$, and $E_{mw}(z)$ propagating perpendicularly to each other, while a weak optical probe field E_p propagates along the z-direction.

Here, each atom has the energy levels denoted as $|g\rangle$, $|e\rangle$, and $|r\rangle$, respectively. An optical probe field at the frequency ω_p drives the transition between $|g\rangle$ and $|e\rangle$, with the corresponding dipole moment μ_{ge}, and Rabi frequency Ω_p. Instead, the control field has a position-dependent Rabi frequency $\Omega_{mw}(l)$, which drives the transition between $|e\rangle$ and $|r\rangle$ with the dipole moment denoted by μ_{er}. Here, the spatial coordinates may be $l = x, y$ for the 2D or $l = x, y, z$ for the 3D case, respectively. For example, the setting for the 3D case is illustrated in Fig. 1(b). The control field excites the atoms to the Rydberg state $|r\rangle$, where the atoms at the positions $\mathbf{r}_i$ and $\mathbf{r}_j$ interact with each other via the van der Waals (vdW) interaction potential, $V(\mathbf{r}_i - \mathbf{r}_j) = C_6/|\mathbf{r}_i - \mathbf{r}_j|^6$, with the vdW coefficient denoted by C_6 [26].

The total Hamiltonian for such a photon–atom interaction in the cascade configuration can be written in the form $H = H_a + H_{af} + H_{\rm vdW}$, with

$$H_a = -\hbar \sum_j^N [\Delta_p \sigma_{ee}^j + \Delta_2 \sigma_{rr}^j], \tag{1}$$

$$H_{af} = -\hbar \sum_j^N [\Omega_p \sigma_{ge}^j + \Omega_{mw}(l)\sigma_{er}^j + \text{H.c.}], \tag{2}$$

$$H_{\rm vdW} = \hbar \sum_{i<j}^N \sigma_{rr}^i \Delta(r_i - r_j)\sigma_{rr}^j, \tag{3}$$

where $\sigma_{\alpha\beta}^j = |\alpha\rangle_{jj}\langle\beta|(|\alpha\rangle, |\beta\rangle = |g\rangle, |e\rangle, \text{or}|r\rangle)$ is the transition operator for the atom at position $\mathbf{r}_j$. Here, we also introduce the one-photon frequency detuning for the probe and control fields: $\Delta_p = \omega_p - \omega_{eg}$ and $\Delta_c = \omega_{mw} - \omega_{re}$, and two-photon detuning: $\Delta_2 = \Delta_p + \Delta_c$. Based on the Hamiltonian given in Eqs. (1)–(3), one can have the equations of motion for the atomic transitions:

$$\dot{\sigma}_{ge}^j = (i\Delta_p - \gamma_{ge})\sigma_{ge}^j + i\Omega_p(\sigma_{gg}^j - \sigma_{ee}^j) + i\Omega_{mw}(l)^*\sigma_{gr}^j, \tag{4}$$

$$\dot{\sigma}_{gr}^j = [i(\Delta_2 - S(\mathbf{r})) - \gamma_{gr}]\sigma_{gr}^j + i\Omega_{mw}(l)\sigma_{ge}^j - i\Omega_p\sigma_{er}^j, \tag{5}$$

$$\dot{\sigma}_{er}^j = i(\Delta_p - S(r) - \gamma_{er})\sigma_{er}^j + i\Omega_{mw}(l)[\sigma_{ee}^j - \sigma_{rr}^j] + i\Omega_p^*\sigma_{gr}^j, \tag{6}$$

where γ_{ge}, γ_{gr}, and γ_{er} are dephasing rates. Here, $S(r)$ accounts for the total vdW force-induced shift of Rydberg state $|r\rangle$ for an atom at the position $\mathbf{r}$, i.e.,

$$S(\mathbf{r}) = \int \rho(\mathbf{r}')V(\mathbf{r} - \mathbf{r}')\sigma_{rr}(\mathbf{r}')\mathrm{d}^3r', \tag{7}$$

with the atomic density denoted by $\rho(\mathbf{r})$. Without considering the vdW interaction, the steady-state solutions for Eqs. (4)–(6) can be obtained in the low-excitation limit, i.e.,

$$\sigma_{ge}^j = \frac{i[\gamma_{gr} - i\Delta_2]\Omega_p}{(\gamma_{eg}^i - i\Delta_p)(\gamma_{rg} - i\Delta_2) + \Omega_{mw}^2(l)}, \tag{8}$$

$$\sigma_{gr}^j = -\frac{\Omega_c\Omega_p}{(\gamma_{ge} - i\Delta_p)(\gamma_{gr} - i\Delta_2) + \Omega_{mw}^2(l)}. \tag{9}$$

Nevertheless, when the vdW interaction is taken into consideration, in general, it is difficult to solve Eqs. (4)–(6) due to integration over all the volume. However, when each superatom has at most one Rydberg excitation within the blockade volume, we can apply a coarse-grained treatment on an ensemble of superatoms within the weak probe-field approximation [26,27]. By considering $\gamma_g \ll \gamma_{eg}$ and $\Delta_p < \gamma_{eg}$, the steady-state population of Rydberg state $\langle\sigma_{rr}\rangle = \sigma_{rg}.\sigma_{gr}$ is

$$\langle\sigma_{rr}\rangle \approx \frac{|\Omega_c|^2|\Omega_p|^2}{|\Omega_c|^4 + \Delta_2^2\gamma_{eg}^2}. \tag{10}$$

Next, we discuss the vdW shift and consider that an atom is in a Rydberg state induces a van der Waals shift on another atom. When the vdW interaction suppresses the excitation of all the atoms in a small volume, $V_{\rm SA}$, we refer these atoms forming a superatom due to the Rydberg blockade effect. The number of atoms in such a superatom is defined as $n_{\rm SA} = \rho(\mathbf{r})V_{\rm SA}$, where $\rho(r)$ is the atomic density. There is only one Rydberg excited atom in each superatom. The total medium can then be treated as the collection of superatoms, and the number of superatoms in volume V is $N_{\rm SA} = \rho_{\rm SA}V$. Then, the total vdW shift at position r can be written as

$$S(\mathbf{r}) = \sum_j^{N_{\rm SA}} V(\mathbf{r} - \mathbf{r}_j)\Sigma_{RR}(\mathbf{r}_j) = \bar{V}\Sigma_{RR}(\mathbf{r}) + s(\mathbf{r}). \tag{11}$$

The first term in the right-hand side shows the excited superatom at the position $\mathbf{r}_j = \mathbf{r}$, i.e., $\Sigma_{RR}(\mathbf{r}) \to 1$. It means that the excited superatom induces a divergent vdW shift when we average over the superatom volume, i.e., $\bar{V} \cong \frac{1}{\rm V}\int_{\rm V}\Delta r'\mathrm{d}^3r' \to \infty$, with the volume of superatom V. As for the second term in the right-hand side of Eq. (11), it gives us the vdW shift outside the volume, which can be approximated as $\langle s(\mathbf{r})\rangle = \frac{w}{8}\langle\Sigma_{RR}(\mathbf{r})\rangle$ by considering a Lorentzian function of population in the Rydberg state, with the half-width in the spectrum denoted by w. To find the analytical expression for $\Sigma_{RR}(r)$, the ground and single collective Rydberg excited states of a superatom can be expressed as

$$|G\rangle = |g_1, g_2, g_3 \ldots, g_{n_{SA}}\rangle, \tag{12}$$

$$|R^{(1)}\rangle = \frac{1}{\sqrt{n_{SA}}} \times \sum_{j}^{n_{SA}} |g_1, g_2, g_3 \ldots r_j \ldots, g_{n_{SA}}\rangle. \tag{13}$$

By considering that initially superatom in state $|G\rangle$, we then obtain superatom operator $\Sigma_{RG} = |G\rangle\langle R^{(1)}|$ as

$$\Sigma_{RG} = \frac{\sqrt{n_{SA}}\Omega_{mw}(l)\Omega_p\Sigma_{GG}}{\Delta_2(i\gamma_{eg} + \Delta_p) - |\Omega_{mw}(l)|^2}. \tag{14}$$

Using the relation $\Sigma_{GG} + \Sigma_{RR} = 1$, the final expression for $\Sigma_{RR} = \Sigma_{RG}.\Sigma_{GR}$ takes the form

$$\Sigma_{RR} = \frac{n_{SA}|\Omega_{mw}(l)|^2|\Omega_p|^2}{\Upsilon + \gamma_{ge}^2\Delta_2^2}, \tag{15}$$

with $\Upsilon = |\Omega_{mw}(l)|^2|\Omega_p|^2 n_{SA} + [|\Omega_{mw}(l)|^2 - \Delta_p\Delta_2]^2$.

As the optical susceptibility (χ_p) of probe field can be calculated from the transition dipole σ_{ge}, we have

$$\chi_p = \beta\left[\Sigma_{RR}\frac{i\gamma_{eg}}{\gamma_{eg} - i\Delta_p} + [1 - \Sigma_{RR}] \times \frac{i\gamma_{eg}}{\gamma_{eg} - i\Delta_p + |\Omega_{mw}(l)|^2[\gamma_{gr} - i(\Delta_2 - \langle s\rangle)]^{-1}}\right], \tag{16}$$

with the coefficient $\beta = \frac{n|\mu_{ge}|^2}{\hbar\epsilon_0\gamma_{ge}}$ and the number density of atomic medium n. In the following, through the absorption spectrum of the probe field, i.e., Im[χ], one can find the probability distribution of the superatom.

3. RESULTS AND DISCUSSION

As a possible candidate to realize our scheme, we take ^{87}Rb atoms as our atomic species. By taking the transitions $|g\rangle = 5S_{1/2}|F = 2, m_F = 2\rangle$, $|e\rangle = 5F_{3/2}|F = 3, m_F = 3\rangle$, and $|r\rangle = 60S_{1/2}$, we have the parameters $\gamma_{ge} = 3$ MHz, $\gamma_{gr} = 0.02$ MHz, and $C_6 = 1.4 \times 10^{11}$ s^{-1} μm^6. Moreover, if all the atoms are considered as a single superatom [31], one can further set the small frequency shift to zero, i.e., $\langle s\rangle = 0$. Based on Eq. (16), when the control field is a position-dependent function, we can retrieve the corresponding position information of Rydberg superatoms. In particular, pairs of standing waves are applied as the position-dependent function for the control field.

A. 2D Localization

In this section, we analyze the conditional position probability distribution of the Rydberg superatom in 2D space, i.e., the x–y plane. To have 2D localization of Rydberg superatoms, the control microwave wave is applied in the standing-wave function, which is a superposition of two orthogonal standing waves along the x- and y-directions. Here, the position-dependent Rabi frequency $\Omega_{mw}(x, y)$ for the control field has the form

$$\Omega_{mw}(x, y) = \Omega_1(x) + \Omega_2(y), \tag{17}$$

with

$$\Omega_1(x) = \Omega_1[\sin(\kappa_1 x + \zeta) + \sin(\kappa_2 x)], \tag{18}$$

$$\Omega_2(y) = \Omega_2[\sin(\kappa_3 y + \xi) + \sin(\kappa_4 y)], \tag{19}$$

where $\kappa_i = 2\pi/\lambda_i (i = 1, 2, 3, 4)$ is the corresponding wave vector at the wavelength $\lambda_i (i = 1, 2, 3, 4)$. Moreover, the parameters ζ and ξ are the associated phase shifts.

To investigate the effect of detuning in the probe frequency Δ_p and phase shifts in the microwave standing waves on the precision position measurement of superatoms, we start our analysis by considering all the standing waves having the same wavelengths, i.e., $\kappa_1 = \kappa_2 = \kappa_3 = \kappa_4 = \kappa$, and setting the phase shifts equal to zero, i.e., $\zeta = \xi = 0$.

In Fig. 2, we plot the 2D conditional position probability distribution, defined as $W(x, y) \propto \mathrm{Im}[\chi]$, which can be obtained through the absorption in the probe field; see Eq. (16). In terms of the normalized coordinates κx and κy, four different values of probe field detuning are depicted, i.e., (a) and (b) $\Delta_p = 0$, (c) and (d) $\Delta_p = 10\Gamma$, (e) and (f) $\Delta_p = 20\Gamma$, and (g) and (h) $\Delta_p = 24\Gamma$, with the scaling parameter Γ setting to 1 MHz. Here, one can find the intensity plots

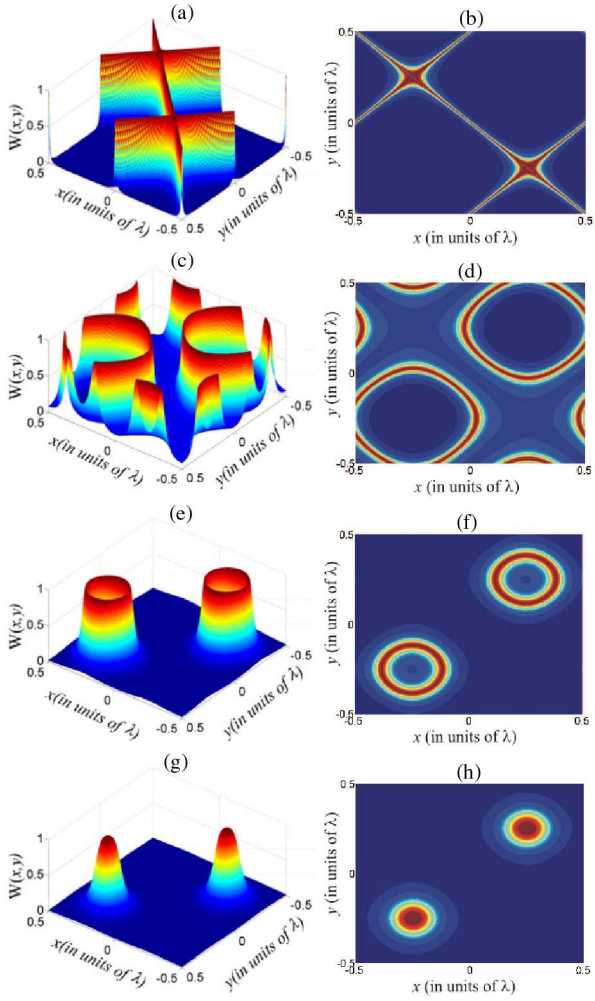

Fig. 2. Conditional position probability distribution $W(x, y)$ in the normalized coordinates x and y for different values of probe detuning: (a),(b) $\Delta_p = 0$; (c),(d) $\Delta_p = 10\Gamma$; (e),(f) $\Delta_p = 20\Gamma$; and (g), (h) $\Delta_p = 24\Gamma$. Here, the intensity plots are shown in the left panel, while the corresponding contour plots are shown in the right panel. Other parameters used are $\Omega_1 = \Omega_2 = \Omega = 6\Gamma$, $\Omega_p = 0.1\Gamma$, $\Delta_c = 0$, $\kappa_1 = \kappa_2 = \kappa_3 = \kappa_4 = \kappa$, $\zeta = \xi = 0$, $\gamma_{ge} = 3\Gamma$, $\gamma_{gr} = 0.02\Gamma$, and $n_{SA} = 15$, respectively.

shown in the left panel and the corresponding contour plots in the right panel.

When the probe detuning is zero $\Delta_p = 0$, we can see that the superatom is uniformly distributed on the diagonals of four quadrants, as shown in Figs. 2(a) and 2(b). In this scenario, the 2D conditional position probability distribution $W(x, y)$ cannot give us any information about the position of superatoms. However, as the probe field detuning increases to $\Delta_p = 10\Gamma$, while keeping the other parameters fixed, the location of maximal values in $W(x, y)$ changes accordingly. In particular, the superatom will be mainly localized in the first and third quadrants in this x–y plane when $\Delta_p = 10\Gamma$; see Figs. 2(c) and 2(d). As shown in Figs. 2(e) and 2(d), two crater-like structures appear in the first and third quadrants when $\Delta_p = 20\Gamma$. Now, the superatom is localized along the rings of these crater-like structures. However, the position information of superatoms is still ambiguous. The precision in position information can be enhanced by further increasing the probe field detuning. When the probe detuning is $\Delta_p = 24\Gamma$, as shown in Figs. 2(g) and 2(h), we have spike-like patterns located at the first and third quadrants. It means that one can obtain two well-defined positions of superatoms at the position $(\kappa x, \kappa y) = (\pm\pi/2, \pm\pi/2)$.

Based on the results shown in Fig. 2, one can see that the probe field detuning plays an important role in the precision of position measurement on Rydberg superatoms. Nevertheless, due to the periodicity associated with standing waves, there are always two possible positions of superatoms with the same maximal value in a single measurement. To obtain a single maximal value on the position information of superatoms, we borrow the results from previous studies [40,47–49]. It is known that the phase shifts also play an important role in the reduction of localization peaks. Then, in Fig. 3, we study the phase shifts of standing waves on the 2D conditional position probability distribution $W(x, y)$. We also assume slightly different wavelengths of the two standing-wave fields having wave vectors κ_1 and κ_3. The corresponding frequencies will also change and the fields will slightly detune from the transition. The position-dependent Rabi frequency takes the form $\Omega_{mw}(x,y) = \Omega_1' e^{\delta_1 t}\sin(\kappa_1 x + \zeta) + \Omega_1 \sin(\kappa_2 x) + \Omega_2' e^{\delta_2 t}\sin(\kappa_3 y + \xi) + \Omega_2 \sin(\kappa_4 y)$ with $\delta_1 = \omega_1 - \omega_{re}$ and $\delta_2 = \omega_2 - \omega_{re}$ the detunings of the first and third microwave fields. The net detuning is defined as $\Delta_c = \omega_{mw} - \omega_{re}$, where $\omega_{mw} = (\omega_1 + \omega_1)/2$. We consider small change in wavelength and hence δ_1, δ_2, and Δ_c are very small and their overall impact on the system is negligible. Therefore, in the following discussion we ignore δ_1, δ_2, and Δ_c.

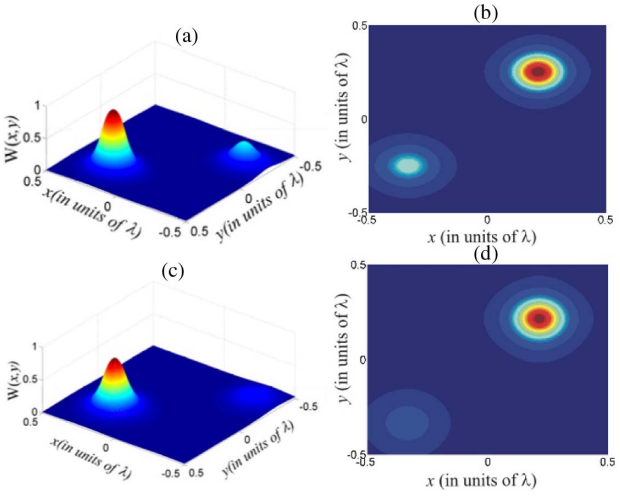

Fig. 3. Conditional position probability distribution $W(x, y)$ in the normalized coordinates x and y for (a),(b) $\kappa_1 = 0.8\kappa$, $\zeta = \pi/4$; and (c),(d) $\kappa_1 = \kappa_3 = 0.8\kappa$, $\zeta = \xi = \pi/4$. The other parameters used are the same as those in Fig. 2(g).

When we change the wavelength of the first standing wave to $\kappa_1 = 0.8\kappa$, along with the corresponding phase shift $\zeta = \pi/4$, as shown in Figs. 3(a) and 3(b), now the symmetry in the resulting conditional position probability distribution breaks. As one can see, the height of the peak located at $(\kappa x, \kappa y) = (-\pi/2, -\pi/2)$ decreases considerably. Now, the probability of finding the superatom in the first quadrant is much higher than that in the third quadrant. Moreover, when we choose $\kappa_1 = \kappa_3 = 0.8\kappa$ and $\zeta = \xi = \pi/4$ [see Figs. 3(c) and 3(d)], one can obtain a single position information of superatom in the first quadrant at $(\pi/2, \pi/2)$.

B. 3D Localization

To extend our proposed scheme to 3D localization of Rydberg superatoms, we utilize the control field in the superposition of three orthogonal pairs of standing waves along the x, y, and z directions. Explicitly, we define the Rabi frequency for the control field having the form

$$\Omega_{mw}(x, y, z) = \Omega_1(x) + \Omega_2(y) + \Omega_3(z), \tag{20}$$

where $\Omega_1(x)$ and $\Omega_2(y)$ are the same as those given in Eqs. (18)–(19), while the third one $\Omega_3(z)$ has the form

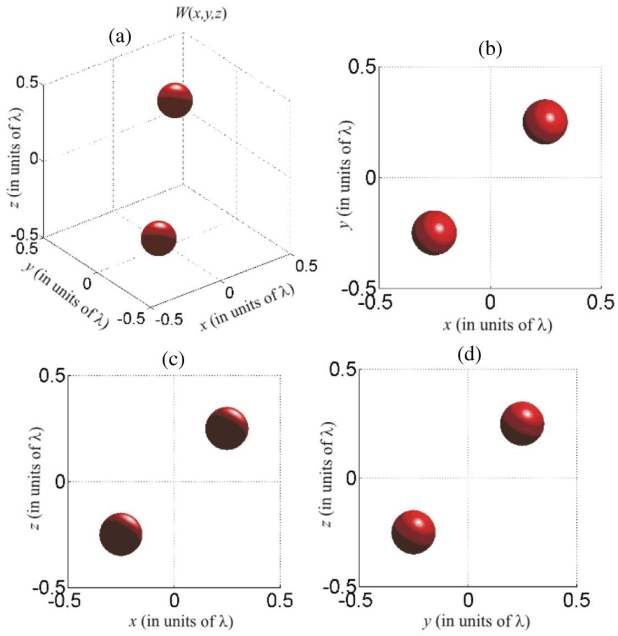

Fig. 4. (a) 3D conditional position probability distribution $W(x, y, z)$ in the normalized coordinates x, y, and z, with the corresponding 2D view in (b)–(d) along the x–y, x–z, and y–z cross sections, respectively. The parameters used are $\kappa_1 = \kappa_2 = \kappa_3 = \kappa_4 = \kappa_5 = \kappa_6 = \kappa$, $\zeta = \xi = \phi = 0$, $\Omega_1 = \Omega_2 = \Omega_3 = 4\Gamma$, $\Omega_p = 0.1\Gamma$, $\Delta_p = 24\Gamma$, $\Delta_c = 0$, $\gamma_{ge} = 3\Gamma$, $\gamma_{gr} = 0.02\Gamma$, and $n_{sa} = 15$.

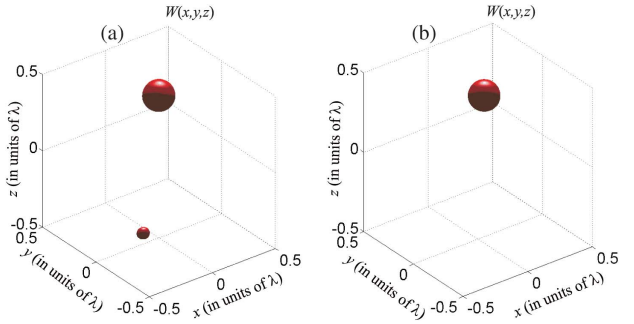

Fig. 5. 3D conditional position probability distribution $W(x, y, z)$ in the normalized coordinates x, y, and z for (a) $\kappa_1 = 0.8\kappa$, $\zeta = \pi/4$, and (b) $\kappa_1 = \kappa_3 = \kappa_5 = 0.8\kappa$, $\zeta = \xi = \phi = \pi/4$. The other parameters used are the same as those in Fig. 4.

$$\Omega_3(z) = \Omega_3[\sin(\kappa_5 z + \phi) + \sin(\kappa_6 z)]. \quad (21)$$

Here, the phase shift ϕ is associated with the standing wave in the wave vector κ_5.

In Fig. 2(c), we obtained the two possible positions of the superatom at $(\kappa x, \kappa y) = (\pm\pi/2, \pm\pi/2)$ with the best spatial resolution. To convert it into 3D, we plot the isosurfaces for $W(x, y, z) = 0.5$ that corresponds to the full width at half-maximum; see Fig. 4. The size of the sphere shows the probability of finding the superatom. As the scenario in 2D, the position information of the superatom in 3D remains ambiguous without the introduction of phase shifts, as illustrated in Fig. 4. To have a single position information of superatoms, we introduce phase shifts to the standing waves for slightly different wavelengths. As shown in Fig. 5(a), the values of position probability distribution $W(x, y, z)$ at $(\kappa x, \kappa y, \kappa z) = (-\pi/2, -\pi/2, -\pi/2)$ significantly decrease with a phase shift, i.e., for $\kappa_1 = 0.8\kappa$ and $\zeta = \pi/4$. With a suitable set of phase shifts, such as $\kappa_1 = \kappa_3 = \kappa_5 = 0.8\kappa$ and $\zeta = \xi = \phi = \pi/4$, we can obtain an almost perfect single peak only located at $(\pi/2, \pi/2, \pi/2)$ in 3D space, as shown in Fig. 5(b). Now, the location of Rydberg superatoms can be achieved at the sub-microwave wavelength scale.

4. CONCLUSION

In conclusion, by utilizing pairs of standing microwaves, we study the 2D and 3D atomic localization of superatoms in the configuration of Rydberg-dressed electromagnetically induced transparency. With a suitable phase shift associated with the standing microwaves, as well as the probe field detuning, a single position of Rydberg superatoms can be obtained with the precision at the sub-microwave wavelength by measuring the absorption spectrum from the optical probe field. By taking ^{87}Rb atoms as the candidate to implement, our results demonstrate the possibility for atomic localization in the Rydberg superatoms.

REFERENCES

1. M. D. Lukin, M. Fleischhauer, R. Cote, L. M. Duan, D. Jaksch, J. I. Cirac, and P. Zoller, "Dipole blockade and quantum information processing in mesoscopic atomic ensembles," Phys. Rev. Lett. **87**, 037901 (2001).
2. D. Jaksch, J. I. Cirac, P. Zoller, S. L. Rolston, R. Cote, and M. D. Lukin, "Fast quantum gates for neutral atoms," Phys. Rev. Lett. **85**, 2208–2211 (2000).
3. D. Moller, L. B. Madsen, and K. Molmer, "Quantum gates and multiparticle entanglement by Rydberg excitation blockade and adiabatic passage," Phys. Rev. Lett. **100**, 170504 (2008).
4. M. Muller, I. Lesanovsky, H. Weimer, H. P. Buchler, and P. Zoller, "Mesoscopic Rydberg gate based on electromagnetically induced transparency," Phys. Rev. Lett. **102**, 170502 (2009).
5. L. Isenhower, E. Urban, X. L. Zhang, A. T. Gill, T. Henage, T. A. Johnson, T. G. Walker, and M. Saffman, "Demonstration of a neutral atom controlled-NOT quantum gate," Phys. Rev. Lett. **104**, 010503 (2010).
6. K. Hammerer, A. S. Sorensen, and E. S. Polzik, "Quantum interface between light and atomic ensembles," Rev. Mod. Phys. **82**, 1041–1093 (2010).
7. A. E. B. Nielsen and K. Molmer, "Deterministic multimode photonic device for quantum-information processing," Phys. Rev. A **81**, 043822 (2010).
8. D. Petrosyan and M. Fleischhauer, "Quantum information processing with single photons and atomic ensembles in microwave coplanar waveguide resonators," Phys. Rev. Lett. **100**, 170501 (2008).
9. T. E. Lee, H. Haffner, and M. C. Cross, "Collective quantum jumps of Rydberg atoms," Phys. Rev. Lett. **108**, 023602 (2012).
10. A. V. Gorshkov, R. Nath, and T. Pohl, "Dissipative many-body quantum optics in Rydberg media," Phys. Rev. Lett. **110**, 153601 (2013).
11. H. Weimer, M. Muller, I. Lesanovsky, P. Zoller, and H. P. Buchler, "A Rydberg quantum simulator," Nat. Phys. **6**, 382–388 (2010).
12. D. Tong, S. M. Farooqi, J. Stanojevic, S. Krishnan, Y. P. Zhang, R. Cote, E. E. Eyler, and P. L. Gould, "Local blockade of Rydberg excitation in an ultracold gas," Phys. Rev. Lett. **93**, 063001 (2004).
13. K. Singer, M. Reetz-Lamour, T. Amthor, L. G. Marcassa, and M. Weidemüller, "Suppression of excitation and spectral broadening induced by interactions in a cold gas of Rydberg atoms," Phys. Rev. Lett. **93**, 163001 (2004).
14. E. Urban, T. A. Johnson, T. Henage, L. Isenhower, D. D. Yavuz, T. G. Walker, and M. Saffman, "Observation of Rydberg blockade between two atoms," Nat. Phys. **5**, 110–114 (2009).
15. C. S. Hofmann, G. Gunter, H. Schempp, M. Robert-de-Saint-Vincent, M. Gärttner, J. Evers, S. Whitlock, and M. Weidemüller, "Sub-Poissonian statistics of Rydberg-interacting dark-state polaritons," Phys. Rev. Lett. **110**, 203601 (2013).
16. R. Heidemann, U. Raitzsch, V. Bendkowsky, B. Butscher, R. Löw, L. Santos, and T. Pfau, "Evidence for coherent collective Rydberg excitation in the strong blockade regime," Phys. Rev. Lett. **99**, 163601 (2007).
17. Y. O. Dudin, L. Li, F. Bariani, and A. Kuzmich, "Observation of coherent many-body Rabi oscillations," Nat. Phys. **8**, 790–794 (2012).
18. A. Gaetan, Y. Miroshnychenko, T. Wilk, A. Chotia, M. Viteau, D. Comparat, P. Pillet, A. Browaeys, and P. Grangier, "Observation of collective excitation of two individual atoms in the Rydberg blockade regime," Nat. Phys. **5**, 115–118 (2009).
19. J. Honer, R. Low, H. Weimer, T. Pfau, and H. P. Buchler, "Artificial atoms can do more than atoms: deterministic single photon subtraction from arbitrary light fields," Phys. Rev. Lett. **107**, 093601 (2011).
20. T. Peyronel, O. Firstenberg, Q.-Y. Liang, S. Hofferberth, A. V. Gorshkov, T. Pohl, M. D. Lukin, and V. Vuletic, "Quantum nonlinear optics with single photons enabled by strongly interacting atoms," Nature (London) **488**, 57–60 (2012).
21. S. Baur, D. Tiarks, G. Rempe, and S. Durr, "Single-photon switch based on Rydberg blockade," Phys. Rev. Lett. **112**, 073901 (2014).
22. T. Pohl, E. Demler, and M. D. Lukin, "Dynamical crystallization in the dipole blockade of ultracold atoms," Phys. Rev. Lett. **104**, 043002 (2010).
23. A. K. Mohapatra, T. R. Jackson, and C. S. Adams, "Coherent optical detection of highly excited Rydberg states using electromagnetically induced transparency," Phys. Rev. Lett. **98**, 113003 (2007).
24. A. K. Mohapatra, M. G. Bason, B. Butscher, K. J. Weatherill, and C. S. Adams, "A giant electro-optic effect using polarizable dark state," Nat. Phys. **4**, 890–894 (2008).
25. J. D. Pritchard, D. Maxwell, A. Gauguet, K. J. Weatherill, M. P. A. Jones, and C. S. Adams, "Cooperative atom-light interaction in a blockaded Rydberg ensemble," Phys. Rev. Lett. **105**, 193603 (2010).

26. D. Petrosyan, J. Otterbach, and M. Fleischhauer, "Electromagnetically induced transparency with Rydberg atoms," Phys. Rev. Lett. **107**, 213601 (2011).
27. Y.-M. Liu, D. Yan, X.-D. Tian, C.-L. Cui, and J.-H. Wu, "Electromagnetically induced transparency with cold Rydberg atoms: superatom model beyond the weak-probe approximation," Phys. Rev. A **89**, 033839 (2014).
28. C. Ates, S. Sevinli, and T. Pohl, "Electromagnetically induced transparency in strongly interacting Rydberg gases," Phys. Rev. A **83**, 041802 (2011).
29. Ziauddin, Y.-L. Chuang, and R.-K. Lee, "PT-symmetry in Rydberg atoms," Europhys. Lett. **115**, 14005 (2016).
30. A. Carmele, B. Vogell, K. Stannigel, and P. Zoller, "Opto-nanomechanics strongly coupled to a Rydberg superatom: coherent versus incoherent dynamics," New J. Phys. **16**, 063042 (2014).
31. D. Yan, Z. H. Wang, C. N. Ren, H. Gao, Y. Li, and J. Wu, "Duality and bistability in an optomechanical cavity coupled to a Rydberg superatom," Phys. Rev. A **91**, 023813 (2015).
32. A. M. Herkommer, W. P. Schleich, and M. S. Zubairy, "Autler-Townes microscopy on a single atom," J. Mod. Opt. **44**, 2507–2513 (1997).
33. S. Qamar, S. Y. Zhu, and M. S. Zubairy, "Precision localization of single atom using Autler-Townes microscopy," Opt. Commun. **176**, 409–416 (2000).
34. S. Qamar, S. Y. Zhu, and M. S. Zubairy, "Atom localization via resonance fluorescence," Phys. Rev. A **61**, 063806 (2000).
35. E. Paspalakis and P. L. Knight, "Localizing an atom via quantum interference," Phys. Rev. A **63**, 065802 (2001).
36. F. Ghafoor, S. Qamar, and M. S. Zubairy, "Atom localization via phase and amplitude control of the driving field," Phys. Rev. A **65**, 043819 (2002).
37. M. Sahrai, H. Tajalli, K. T. Kapale, and M. S. Zubairy, "Subwavelength atom localization via amplitude and phase control of the absorption spectrum," Phys. Rev. A **72**, 013820 (2005).
38. K. T. Kapale and M. S. Zubairy, "Subwavelength atom localization via amplitude and phase control of the absorption spectrum. II," Phys. Rev. A **73**, 023813 (2006).
39. S. Qamar, J. Evers, and M. S. Zubairy, "Atom microscopy via two-photon spontaneous emission spectroscopy," Phys. Rev. A **79**, 043814 (2009).
40. S. Qamar, A. Mehmood, and S. Qamar, "Subwavelength atom localization via coherent manipulation of the Raman gain process," Phys. Rev. A **79**, 033848 (2009).
41. V. Ivanov and Y. Rozhdestvensky, "Two-dimensional atom localization in a four-level tripod system in laser fields," Phys. Rev. A **81**, 033809 (2010).
42. C. Ding, J. Li, Z. Zhan, and X. Yang, "Two-dimensional atom localization via spontaneous emission in a coherently driven five-level M-type atomic system," Phys. Rev. A **83**, 063834 (2011).
43. C. Ding, J. Li, R. Yu, X. Hao, and Y. Wu, "High-precision atom localization via controllable spontaneous emission in a cycle-configuration atomic system," Opt. Express **20**, 7870–7885 (2012).
44. C. Ding, J. Li, X. Yang, D. Zhang, and H. Xiong, "Proposal for efficient two-dimensional atom localization using probe absorption in a microwave-driven four-level atomic system," Phys. Rev. A **84**, 043840 (2011).
45. R. G. Wan and T. Y. Zhang, "Two-dimensional sub-half-wavelength atom localization via controlled spontaneous emission," Opt. Express **19**, 25823–25832 (2011).
46. R. G. Wan, T. Y. Zhang, and J. Kou, "Two-dimensional sub-half-wavelength atom localization via phase control of absorption and gain," Phys. Rev. A **87**, 043816 (2013).
47. Rahmatullah and S. Qamar, "Two-dimensional atom localization via probe-absorption spectrum," Phys. Rev. A **88**, 013846 (2013).
48. Rahmatullah, A. Wahab, and S. Qamar, "Precision in 2D atom localization via coherent manipulation of the Raman gain process," Laser Phys. Lett. **11**, 045202 (2014).
49. Rahmatullah and S. Qamar, "Two-dimensional atom localization via Raman-driven coherence," Phys. Lett. A **378**, 684–690 (2013).
50. V. Ivanov, Y. Rozhdestvensky, and K. Suominen, "Three-dimensional atom localization by laser fields in a four-level tripod system," Phys. Rev. A **90**, 063802 (2014).
51. Z. Wang and B. Yu, "Efficient three-dimensional atom localization via probe absorption," J. Opt. Soc. Am. B **32**, 1281–1283 (2015).
52. Z. Zhu, W. X. Yang, X. T. Xie, S. Liu, S. Liu, and R. K. Lee, "Three-dimensional atom localization from spatial interference in a double two-level atomic system," Phys. Rev. A **94**, 013826 (2016).
53. Z. Wang, J. Chen, and B. Yu, "High-dimensional atom localization via spontaneously generated coherence in a microwave-driven atomic system," Opt. Express **25**, 3358–3372 (2017).